Cellular clearance of circulating transthyretin decreases cell-nonautonomous proteotoxicity in *Caenorhabditis elegans*

Kayalvizhi Madhivanan[a,b,c], Erin R. Greiner[a,b,c,1], Miguel Alves-Ferreira[a,b,c,d,e,f], David Soriano-Castell[a,b,c], Nirvan Rouzbeh[a,b,c,2], Carlos A. Aguirre[a,b,c], Johan F. Paulsson[a,3], Justin Chapman[g], Xin Jiang[g], Felicia K. Ooi[h], Carolina Lemos[d,e,f], Andrew Dillin[i,j], Veena Prahlad[h], Jeffery W. Kelly[a,k,l], and Sandra E. Encalada[a,b,c,4]

[a]Department of Molecular Medicine, The Scripps Research Institute, La Jolla, CA 92037; [b]Department of Molecular and Cellular Neuroscience, The Scripps Research Institute, La Jolla, CA 92037; [c]Dorris Neuroscience Center, The Scripps Research Institute, La Jolla, CA 92037; [d]Instituto de Biologia Molecular e Celular, Universidade do Porto, 4150-171 Porto, Portugal; [e]Instituto de Investigação e Inovação em Saúde, Universidade do Porto, 4150-171 Porto, Portugal; [f]Instituto de Ciências Biomédicas de Abel Salazar, Universidade do Porto, 4150-171 Porto, Portugal; [g]Misfolding Diagnostics, San Diego, CA 92121; [h]Department of Biology, Aging Mind and Brain Initiative, University of Iowa, Iowa City, IA 52242; [i]Department of Molecular and Cell Biology, University of California, Berkeley, CA 94720; [j]Howard Hughes Medical Institute, University of California, Berkeley, CA 94720; [k]Department of Chemistry, The Scripps Research Institute, La Jolla, CA 92037; and [l]The Skaggs Institute for Chemical Biology, The Scripps Research Institute, La Jolla, CA 92037

Edited by F. Ulrich Hartl, Max Planck Institute of Biochemistry, Martinsried, Germany, and approved July 6, 2018 (received for review February 7, 2018)

Cell-autonomous and cell-nonautonomous mechanisms of neurodegeneration appear to occur in the proteinopathies, including Alzheimer's and Parkinson's diseases. However, how neuronal toxicity is generated from misfolding-prone proteins secreted by nonneuronal tissues and whether modulating protein aggregate levels at distal locales affects the degeneration of postmitotic neurons remains unknown. We generated and characterized animal models of the transthyretin (TTR) amyloidoses that faithfully recapitulate cell-nonautonomous neuronal proteotoxicity by expressing human TTR in the *Caenorhabditis elegans* muscle. We identified sensory neurons with affected morphological and behavioral nociception-sensing impairments. Nonnative TTR oligomer load and neurotoxicity increased following inhibition of TTR degradation in distal macrophage-like nonaffected cells. Moreover, reducing TTR levels by RNAi or by kinetically stabilizing natively folded TTR pharmacologically decreased TTR aggregate load and attenuated neuronal dysfunction. These findings reveal a critical role for *in trans* modulation of aggregation-prone degradation that directly affects postmitotic tissue degeneration observed in the proteinopathies.

aggregation | cell-nonautonomous | neurodegeneration | nonnative oligomers | polyneuropathy

In protein-aggregation disorders, cell-autonomous and cell-nonautonomous mechanisms of neurodegeneration appear to occur, the latter associated with the propagation of protein aggregates and/or pathologies throughout the nervous system (1, 2). Elucidating these degenerative pathways is often confounded by the fact that affected tissues express the misfolding-prone protein(s). Moreover, it is unclear whether modulating levels of native aggregation-prone proteins or of protein aggregates in distal tissues would change cell-nonautonomous proteotoxicity. Knowledge of these features is important for further understanding neurodegenerative diseases and for envisioning new therapeutic strategies.

In the transthyretin (TTR) systemic amyloidoses, the unaffected liver secretes tetrameric TTR into the blood stream, where TTR dissociates, misfolds and aggregates, compromising organ systems such as the heart and the autonomic and peripheral nervous systems, tissues that do not synthesize TTR (3). Thus, cell-nonautonomous proteotoxic pathways are clearly distinguished in the TTR amyloidoses, allowing the mechanism(s) to be carefully studied. Native TTR exists as a β-sheet–rich tetramer (4), whose established function is to transport holo-retinol–binding protein in the plasma and to serve as a backup carrier for thyroxine (T_4) (5, 6). Strong genetic, pathologic, biochemical, and pharmacologic evidence suggests that TTR amyloid diseases result from TTR aggregation, compromising the function of various tissues (7–10). A central unanswered question is how TTR aggregation leads to the cell-nonautonomous demise of postmitotic tissues, including neurons (11). This key question remains unanswered for all human amyloid diseases (12–14). Moreover, it is unclear whether nonnative (NN) TTR oligomers contribute to neurodegeneration and, if so, whether their levels can be modulated at distal sites to diminish neuronal proteotoxicity (9, 15).

Over 115 different TTR mutations associated with human disease render the tetramer less stable and more aggregation prone (16, 17). The most common TTR variant is V30M (10), which leads to familial amyloid polyneuropathy (FAP), affecting the peripheral and autonomic nervous systems and resulting in the degeneration of thermo- and pain-sensing neurons (18). The

Significance

Evidence suggests that transthyretin (TTR) amyloid diseases result from rate-limiting dissociation of TTR tetramers secreted from the liver into monomers, followed by monomer misfolding and misassembly into a spectrum of aggregates that compromise postmitotic tissue function, including peripheral nerve function. It is unknown how TTR aggregation leads to the demise of neurons cell nonautonomously. Herein we introduce transgenic *Caenorhabditis elegans* models of TTR amyloidosis that exhibit aggregation and quantifiable cell nonautonomous neuronal phenotypes, including impaired pain sensation, as seen in humans, and altered neuronal morphology. Neuronal dysfunction can be exacerbated by eliminating distal macrophage-like cells that degrade TTR and ameliorated by treating the transgenic worms with TTR RNAi or a TTR kinetic stabilizer, strategies that also delay human polyneuropathy.

Author contributions: K.M., E.R.G., J.W.K., and S.E.E. designed research; K.M., E.R.G., M.A.-F., D.S.-C., N.R., C.A.A., J.F.P., J.C., X.J., and F.K.O. performed research; K.M., E.R.G., M.A.-F., N.R., C.A.A., J.F.P., J.C., X.J., and F.K.O. analyzed data; and K.M., E.R.G., C.L., A.D., V.P., J.W.K., and S.E.E. wrote the paper.

Conflict of interest statement: J.W.K. is a consultant for and shareholder in Pfizer, which sells tafamidis.

This article is a PNAS Direct Submission.

[1]Present address: Illumina, San Diego, CA 92122.

[2]Present address: Department of Biomedical and Pharmaceutical Sciences, University of Montana, Missoula, MT 59812.

[3]Present address: Department of Obesity Biology, Global Research, Novo Nordisk A/S, 2760 Måløv, Denmark.

[4]To whom correspondence should be addressed. Email: encalada@scripps.edu.

This article contains supporting information online at www.pnas.org/lookup/suppl/doi:10.1073/pnas.1801117115/-/DCSupplemental.

Published online July 30, 2018.

highly unstable D18G TTR variant is not readily secreted by the liver but instead is targeted for endoplasmic reticulum (ER)-associated degradation (ERAD) (16, 19). Partial secretion of D18G TTR from the choroid plexus results in aggregation that leads to familial meningocerebrovascular amyloidosis characterized by dementia and cerebrovascular bleeding (20). The aggregation of circulating WT TTR leads to senile systemic amyloidosis, a cardiomyopathy that is the most common TTR amyloid disease affecting ∼10% of elderly adults, leading to congestive heart failure (21). Interestingly, mutations also exist that are protective against disease. For example, T119M TTR when present in hetero-allelic combination with V30M TTR results in the formation of highly kinetically stable, non-amyloidogenic T119M/V30M heterotetramers that stop or delay FAP pathology (7).

Numerous attempts to model human neuronal TTR proteotoxicity in transgenic mice have failed to recapitulate cell-nonautonomous disease phenotypes, including degeneration of postmitotic tissue, despite the presence of extracellular TTR aggregates (22). In *Drosophila*, expression of TTR in the cytosol of neurons resulted in neuronally related phenotypes, but in humans TTR is not significantly expressed in the cytosol of neurons (23, 24). Therefore, there is a pressing need to develop an animal model relevant to human pathology wherein the mechanism of TTR aggregation-associated toxicity occurs cell nonautonomously. Successful models become even more relevant if the existing regulatory agency-approved drugs that slow the progression of human FAP, such as tafamidis and patisiran (an RNAi therapeutic targeting TTR) (8), also ameliorate disease phenotypes in the animal model, thus contributing to the identification of mechanisms by which TTR is toxic as well as the means by which toxicity can be ameliorated.

Herein we report animal models in the nematode *Caenorhabditis elegans* that generate TTR aggregates including NN oligomers analogous to those in humans (9, 25). Critically, expression of human TTR (hTTR) uniquely in the body-wall muscle resulted in TTR secretion and aggregation and in cell-nonautonomous structural and functional impairments of sensory nociceptive neurons not expressing TTR. Decreasing TTR levels cell nonautonomously resulted in a reduced NN TTR oligomeric load and a significant amelioration of cell-nonautonomous proteotoxicity. These data suggest that TTR oligomers are likely proteotoxic, as is hypothesized to be the case in humans (9, 25, 26). Notably, the degenerative phenotypes in *C. elegans* linked to TTR proteotoxicity were exacerbated by impairing the turnover of TTR tetramers and oligomers in distal cells, suggesting that increased TTR oligomer levels correlate with enhanced proteotoxicity and that enhancing TTR degradation could be a viable therapeutic strategy. These *C. elegans* models provide a platform to study the mechanism(s) of *in trans* neurodegeneration as well as the influence of cell-nonautonomous TTR degradation and have the potential to provide insights into the etiology of other aging-associated protein-aggregation disorders linked to neurodegeneration such as Alzheimer's disease (AD) and Parkinson's disease (PD).

Results

Generation of *C. elegans* Models Expressing Human TTR Variants. To model TTR proteotoxicity in *C. elegans*, we expressed human WT TTR, V30M TTR, or D18G TTR in the body-wall muscle under the control of the *unc-54* promoter (Fig. 1*A*). We modeled these disease-promoting TTR sequences because earlier work showed that they have diverse stabilities and secretion efficiencies that could allow us to investigate the range of cell-nonautonomous versus cell-autonomous effects (16). We also made a transgenic strain with the protective, non–aggregation-prone T119M mutation (7) that allowed us to scrutinize the hypothesis that the proteotoxic phenotypes observed in the pathogenic strains (see below) were not simply the result of the overexpression of an hTTR sequence. In each model strain, the hTTR signal sequence (SS) (Fig. 1*A*) was included to enable TTR to be inserted into the ER and to target it for secretion (see below). As TTR is a small protein and fusions to GFP or other large fluorescent proteins could significantly impact its folding, assembly, and/or trafficking in the early secretory pathway, the TTR transgenes were not tagged.

To test whether the *C. elegans* strains expressed comparable TTR levels, *TTR* mRNA and TTR protein levels were assessed. *TTR* mRNA levels quantitated from age-synchronized animals peaked at day 1 of adulthood and declined by day 8 for all strains (*SI Appendix*, Fig. S1*A*). Soluble and insoluble TTR protein levels were quantified by Western blot (Fig. 1 *B* and *C*) using antibodies that recognized all four hTTR variants equally (*SI Appendix*, Fig. S1*B*) but did not recognize endogenous *C. elegans* TTR-like proteins in the non-TTR control or TTR strains. Animals expressing stable human variants (i.e., WT TTR, V30M TTR, and T119M TTR) generated comparable levels of soluble TTR protein that peaked in day-1 adult animals in all strains (Fig. 1*B*). TTR was not detected in the insoluble pellet except for V30M TTR, which is the most amyloidogenic of these three sequences (Fig. 1*C*). In contrast, animals expressing the highly unstable and, as shown in humans, poorly secreted D18G TTR displayed very low levels of soluble protein but notably higher levels of insoluble TTR that increased with aging (Fig. 1*C*) (16, 20). Collectively, these data show that the strains generated had comparable levels of *TTR* mRNA and TTR

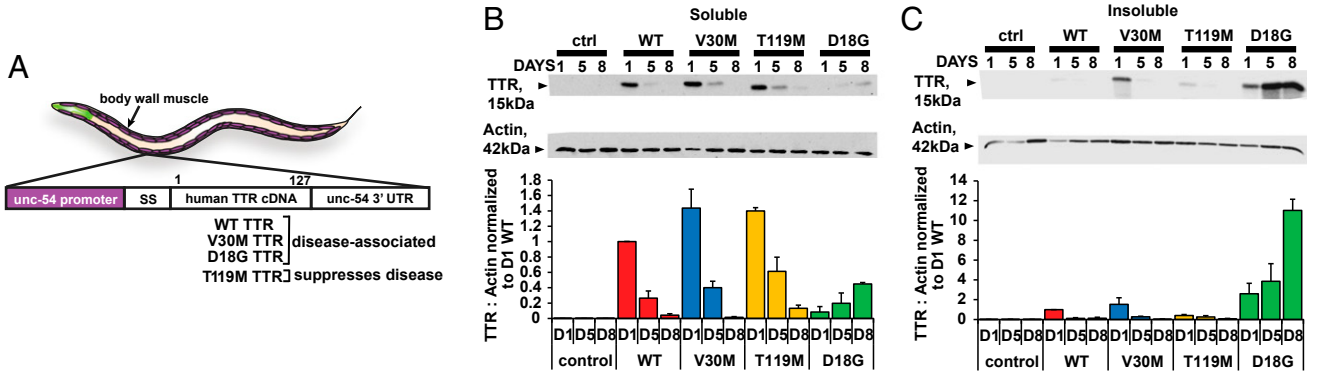

Fig. 1. Generation of *C. elegans* TTR models. (*A*) Schematic of TTR *C. elegans* transgenes generated in this study. The human TTR with SS and full-length WT TTR, V30M TTR, T119M TTR, and D18G TTR variants were expressed under the body-wall muscle–specific promoter *unc-54*. (*B* and *C*, *Upper*) Representative Western blots of soluble (*B*) and insoluble (*C*) fractions of lysates of day-1 (D1), day-5 (D5), and day-8 (D8) adult animals probed with antibody MDX102 against TTR. (*B* and *C*, *Lower*) TTR/actin ratios (mean ± SEM, $n = 3$), aligned to a representative Western blot for one experiment. The percentage difference in soluble TTR/actin ratios between the strains relative to the WT TTR levels in D1 animals are 43%, 39%, and 92% for V30M, T119M, and D18G, respectively. ctrl, control; SS, signal sequence.

protein and that the solubility profile of TTR sequences is consistent with that observed in humans, which had not been previously modeled (16).

Differential Secretion of Tetrameric TTR Variants in *C. elegans* Recapitulates hTTR Secretion Profiles. In humans, WT TTR, V30M TTR, and T119M TTR are efficiently secreted from the liver, while D18G TTR is not (16, 19). To test the hypothesis that hTTR variants expressed in *C. elegans* were secreted from the body-wall muscle with differential secretion efficiencies, we first performed immunofluorescence (IF) with a polyclonal antibody against hTTR to visualize total TTR expression and localization in day-1 adult animals. The TTR signal was observed in the periphery of individual body-wall muscle cells and in colocalization with phalloidin, suggesting that TTR reached the plasma membrane for possible secretion and deposited at myofilament striations of sarcomeres (Fig. 2*A*). In addition, we observed WT, V30M, and T119M TTR signal in the body cavity, demonstrating secretion of TTR from muscle cells. In contrast, the D18G TTR signal was absent from the body cavity, suggesting that this highly unstable variant was not secreted efficiently. Instead, we observed pronounced D18G TTR intracellular aggregates, likely a result of its retention inside muscle cells (Fig. 2*A*). We confirmed these observations by repeating the IF (*SI Appendix*, Fig. S2) using fit-for-purpose antibodies that uniquely and selectively recognized NN TTR (monomers and/or oligomers) but not native TTR tetramers (*SI Appendix*, *SI Materials and Methods* and Fig. S3 *A* and *B*). Whether NN TTR was also present inside other tissues is not clear at this time.

To further scrutinize the hypothesis that natively folded TTR tetramers were secreted from the *C. elegans* body-wall muscle (16), we analyzed their in vivo subcellular localization by feeding animals compound 5 (**CMPD5**) (Fig. 2*B*). This small molecule is a validated fluorogenic probe for natively folded TTR that binds to the T_4-binding sites in TTR and remains dark until it selectively reacts with the Lys-15 ε-amino groups of TTR to render the TTR–(**CMPD5**)$_2$ conjugates fluorescent (27). Pronounced TTR–(**CMPD5**)$_2$ conjugate fluorescence was detected in WT TTR, V30M TTR, and T119M TTR strains in all six coelomocytes, macrophage-like cells that endocytose soluble material from the body cavity for degradation (28) (Fig. 2 *C*, *d*–*l*). These data demonstrate that TTR tetramers were secreted from the muscle. We and others previously observed TTR localization to coelomocytes in independently generated WT TTR *C. elegans* strains (29, 30). Neither the non-TTR control nor the D18G TTR animals showed a TTR–(**CMPD5**)$_2$ conjugate-positive signal in coelomocytes (Fig. 2 *C*, *a*–*c* and *m*–*o*, respectively), suggesting that D18G TTR was not secreted out of muscle cells. Thus, the various TTR sequences expressed in the *C. elegans* body-wall muscle showed secretion

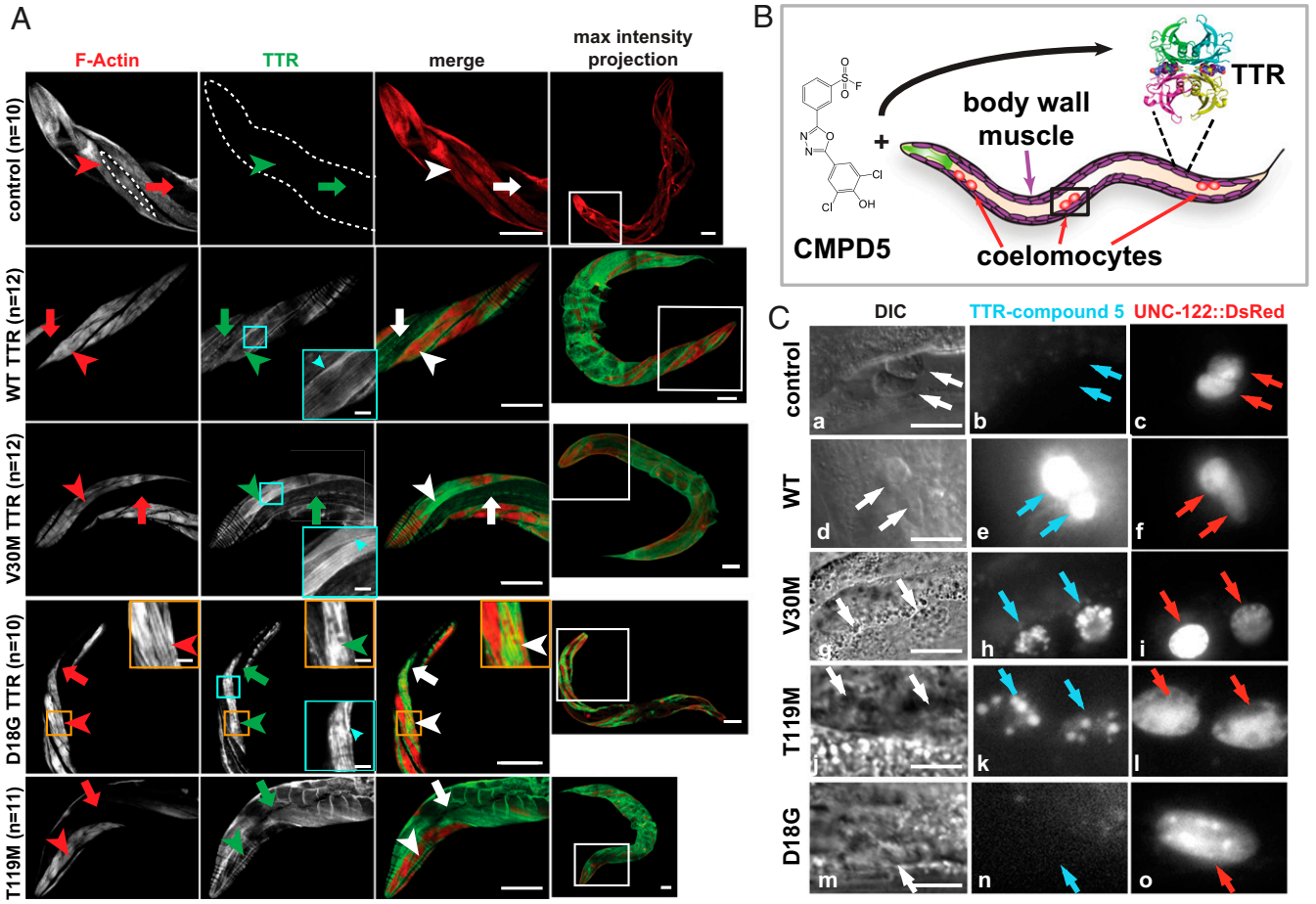

Fig. 2. Differential secretion profiles of *C. elegans* TTR models. (*A*) Representative confocal IF images of adult day-1 animals stained with a polyclonal antibody against TTR (green) and phalloidin (F-actin; red). The panels at the far right show maximal intensity projections of whole animals. *Insets* in white boxes show enlargements of head regions in the adjacent column on the left. Arrowheads point to muscle cells; arrows point to the body cavity. The dotted line in the control F-actin panel outlines the contour of a single body-wall muscle cell. *Insets* in orange boxes show enlargements of aggregates. *Insets* in cyan boxes show enlargements of cell-surface TTR staining. (Scale bars: 50 μm.) (*B*) Schematic diagram of the experiment in which worms were fed **CMPD5** to detect TTR–(**CMPD5**)$_2$ conjugates. The black box shows coelomocytes enlarged in *C*. The pharynx is shown in green. (*C*) Enlargements showing coelomocytes. Arrows point to coelomocytes. Control, $n = 11$; WT, $n = 12$; V30M, $n = 15$; T119M, $n = 21$; D18G, $n = 23$. (Scale bar: 10 μm.) DIC, differential interference contrast microscopy. See also *SI Appendix*, Fig. S2.

profiles comparable to those exhibited by humans, rendering these models suitable for studying TTR cell-nonautonomous proteotoxicity.

Expression of TTR in *C. elegans* Results in the Generation of Native TTR Tetramers and Oligomeric TTR Aggregates. Since soluble and secreted hTTR can remain natively tetrameric or can dissociate, misfold, and aggregate into a variety of aggregate structures, including NN TTR oligomers that we hypothesize are toxic (9, 25), we next characterized the age-dependent profile of tetrameric and oligomeric TTR in the *C. elegans* transgenic TTR strains (25, 31). Natively folded TTR tetramers were quantified in the soluble fractions from lysates of age-synchronized day-1, day-5, and day-8 animals by incubating the lysates with the fluorogenic small molecule **A2** (31). Similar to **CMPD5**, **A2** binds strongly to both T_4-binding pockets of the folded TTR tetramer and reacts with Lys-15 residues to create a fluorescent TTR tetramer–$(\mathbf{A2})_2$ conjugate that is quantified by ultra-performance liquid chromatography (UPLC) (31). Fluorescent TTR tetramer–$(\mathbf{A2})_2$ conjugate levels from *C. elegans* lysates, as measured by UPLC, were compared with a calibrated standard curve generated by the addition of increasing amounts of purified recombinant WT TTR into day-1 control lysates (Fig. 3*A* and *SI Appendix*, Fig. S3*C*). We found that native TTR tetramer levels decreased with aging (Fig. 3*B*). The decrease is consistent with expression of the *unc-54* promoter (32), but message instability, tetramer degradation, or tetramer-to-monomer-to-aggregate conversion could also contribute (16). Notably, the most stable TTR variant (T119M TTR) had the highest TTR tetramer levels from day 1 through day 8 of adulthood, whereas the least stable variant (D18G TTR) yielded the lowest native TTR tetramer levels (Fig. 3*B*), consistent with observations in humans showing that these are highly stable and unstable variants, respectively (16). Thus, the *C. elegans* transgenic strains expressing stable TTR variants generated measurable levels of TTR tetramers.

We next evaluated whether NN oligomeric or aggregated TTR was being generated in the transgenic TTR strains. NN TTR oligomer levels from soluble and insoluble fractions of lysates from all *C. elegans* strains were assessed by Native-PAGE and by a sandwich ELISA using the same antibodies against NN TTR that were used for IF (Fig. 2*A*). Native-PAGE showed the presence of high-molecular-weight aggregates primarily in the soluble and insoluble lysate fractions of the V30M TTR and D18G TTR strains but not in the WT TTR or T119M TTR strains (Fig. 3*C* and *SI Appendix*, Fig. S3*D*). To test whether we could more quantitatively assess NN TTR oligomer levels, soluble and insoluble lysate fractions of day-1 and day-5 age-synchronized animals were analyzed by a sandwich ELISA (*Materials and Methods*) (25). Consistent with the observations from the Native-PAGE analysis (Fig. 3*C*), NN TTR levels were detected primarily in insoluble lysates of D18G TTR strains, but not in lysates from V30M TTR animals (Fig. 3*D*). As with Native-PAGE, the ELISA was unable to detect NN WT TTR or T119M TTR, likely because of the conformational stability of these sequences. The presence of NN oligomers in the transgenic strains expressing V30M TTR and D18G TTR is consistent with the higher amyloidogenicity of these sequences (16). Taken together, these data show that expression of the TTR variants in the *C. elegans* body-wall muscle resulted in the generation of differential native tetramer and NN oligomeric TTR concentrations, as observed in human patients.

TTR FAP Variant Impairs Sensory Nociception Cell Nonautonomously. In FAP patients, the aggregation of V30M TTR and its deposition around peripheral and autonomic neurons is associated with the loss of nociception and temperature perception in the extremities (18). To test whether the expression of V30M TTR in the body-wall muscle leads to the impairment of nociception in *C. elegans*, we measured the reflex-like escape reaction of V30M TTR animals with a thermal-avoidance assay developed previously to measure pain responses (Fig. 4*A*) (33). Individual animal responses were scored into four categories (classes I–IV),

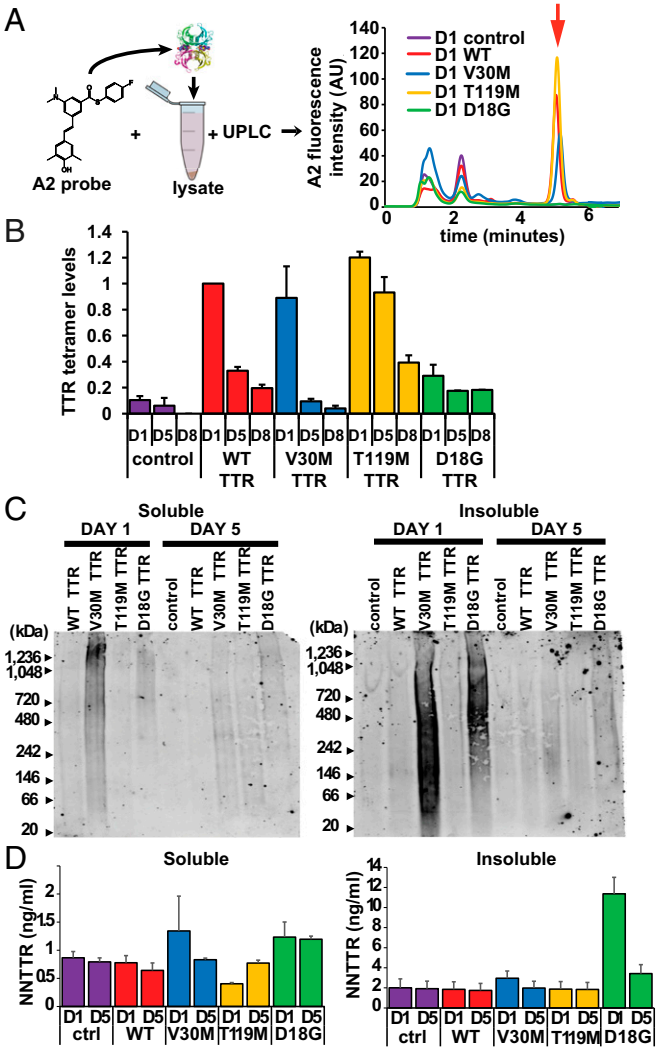

Fig. 3. Soluble and insoluble oligomeric TTR aggregates in *C. elegans* TTR models. (*A*, *Left*) Schematic of the UPLC experiment showing the incubation of **A2** with worm lysates. (*Right*) TTR tetramer–$(\mathbf{A2})_2$ fluorescence chromatograms from the UPLC experiment showing the TTR tetramer elution peak (red arrow) identified as TTR by comparison with recombinant TTR control (*SI Appendix*, Fig. S3*C*). AU, arbitrary units. (*B*) Quantification of TTR tetramer levels from UPLC experiments in *A*. Levels were normalized to those of adult day-1 WT TTR animals (mean ± SEM, $n = 3$). (*C*) Native gel blots of the soluble (*Left*) and insoluble (*Right*) fractions of animal lysates probed with anti-TTR MDX102 antibody. Images are representative of five replicates for day-1 samples and three replicates for day-5 samples. Loading controls are shown in *SI Appendix*, Fig. S3*D*. (*D*) NN TTR quantification by a sandwich ELISA for soluble (*Left*) and insoluble (*Right*) lysate fractions (mean ± SEM, $n = 3$). ctrl, control. See also *SI Appendix*, Fig. S3.

as previously established (*SI Appendix*, *SI Materials and Methods*) (33). As controls, we scored thermal avoidance in *eat-4(n2474)* and *unc-86(n846)* 1-d-old mutant animals, shown previously to have attenuated and unaltered responses, respectively (Fig. 4*B*) (33). A significantly higher percentage of V30M TTR animals (10 ± 0.6%) than non-TTR control animals (0%) or T119M TTR animals (0%) were unresponsive to noxious heat (class IV) (Fig. 4*B* and *SI Appendix*, Table S1). The T119M TTR data demonstrate that the nociceptive defect was not due simply to the overexpression of an hTTR sequence. To ascertain that the V30M TTR-dependent defect was not the result of locomotion-related impairments that would prevent the animals from backing up, we tested reversal movement in each class IV animal with

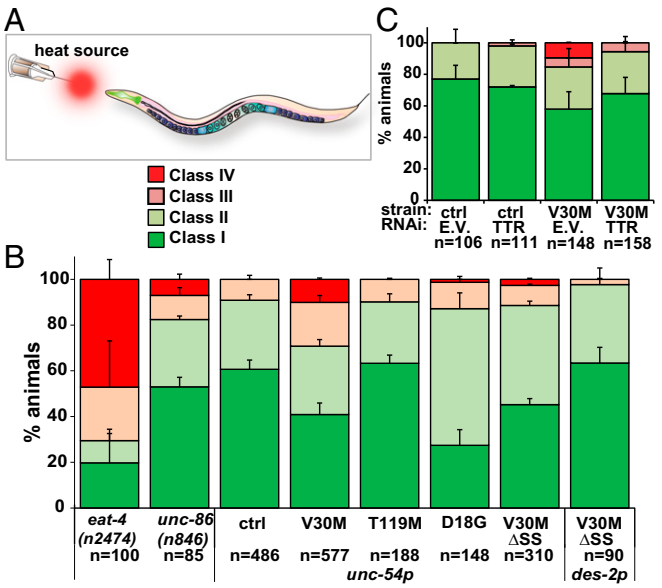

Fig. 4. Cell-nonautonomous nociception impairments of TTR animals. (*A*) Schematic of the thermal-avoidance (nociception) assay. (*B*) Thermal-avoidance response of indicated strains. (*C*) Thermal-avoidance response of indicated strains. *unc-54p* and *des-2p* are body-wall muscle and FLP/PVD neuron promoters, respectively. Data in all graphs are representative of at least two experiments (mean ± SEM). ctrl, control; E.V., empty vector. See also *SI Appendix*, Figs. S4–S6 and Tables S1 and S2 for statistics.

a soft touch to the nose. All class IV animals (100%; $n = 41$) backed in response to this stimulus. To test whether the nociception defects were TTR dependent, we repeated the noxious heat assay in V30M TTR animals treated with TTR RNAi, which afforded a protein knockdown of >90% (*SI Appendix*, Fig. S4). The nociception defect was rescued in RNAi-treated V30M TTR animals (Fig. 4*C* and *SI Appendix*, Table S2). These results are consistent with cell-nonautonomous V30M TTR neuronal toxicity.

To further test whether defects in nociception exhibited by V30M TTR animals were cell nonautonomous, we generated transgenic animals expressing V30M TTR in the body-wall muscle but lacking the SS (V30MΔSS TTR, *SI Appendix*, Fig. S6 *A* and *B*) to prevent its secretion (*SI Appendix*, Fig. S6*C*). V30M ΔSS animals did not exhibit a defective thermal-avoidance response (2.6 ± 0.5% class IV) compared with V30M animals with TTR fused to an SS (10 ± 0.6%) (Fig. 4*B* and *SI Appendix*, Table S1). Furthermore, we tested for thermal avoidance in day-1 D18G TTR animals in which we did not find evidence for TTR secretion (Fig. 2 *A* and *C*). D18G TTR animals did not exhibit defective nociception (Fig. 4*B*). Taken together our data show that secretion of V30M TTR from the muscle results in proteotoxicity to sensory pain-sensing neurons in a cell-nonautonomous manner, likely owing to V30M TTR's ability to dissociate, misfold, and misassemble (16).

Impaired Dendritic Morphology of Somatosensory Neurons in V30M TTR Animals. The neural circuitry for the nociceptive thermal-avoidance responses in *C. elegans* tested here was previously mapped to the AFD and FLP head sensory neurons (33, 34). The FLP neurons are polymodal cells that extend elaborate dendritic branches enveloping the head of the animal (Fig. 5 *A* and *B*) (35). To probe whether the nociceptive defects observed in V30M TTR animals (Fig. 4) correlated with morphological neuronal defects, we quantified the dendritic morphology of their FLP neurons. Day-1 adult V30M TTR animals had a significantly higher number of quaternary branches than age-matched non-TTR control or T119M TTR animals, suggesting that the expression of V30M TTR affects dendritic outgrowth (Fig. 5 *B* and *C*). As extension of quaternary branches toward the hypodermis is critical for FLP sensory function (35), we also quantified the FLP quaternary branch extension angle from the tertiary branch (Fig. 5*D*). V30M TTR animals had quaternary branches that bent backward toward tertiary branches more often than non-TTR control and T119M TTR animals (Fig. 5*E* and *SI Appendix*, Table S3). These data show that sensory endings do not extend fully and in some cases nearly reverse in V30M TTR animals. To test whether these phenotypes were due to developmental defects, we first surveyed the number of quaternary branches in the last larval L4 stage, when FLP quaternary branching is finalizing its development (35). The number of FLP quaternary dendritic branches was lower in L4 non-TTR control larvae than in non-TTR control day-1 adults, showing that quaternary branches are still being added as control animals develop (Fig. 5*C* and *SI Appendix*, Fig. S7*A*). Expression of V30M TTR or T119M TTR resulted in a higher number of quaternary branches in L4 animals than in control animals (*SI Appendix*, Fig. S7*A*). However, the number of branches in T119M TTR L4 larvae as they grew to day-1 adults was similar to those of non-TTR controls, whereas V30M TTR animals continued adding quaternary branches as they transitioned to day-1 adults (Fig. 5*C*). Thus, expression of V30M TTR resulted in ectopic branching in young-adult animals compared with L4 larvae. No significant differences in quaternary FLP branch angle in L4 larvae were observed in non-TTR control, V30M TTR, and T119M TTR transgenic animals, demonstrating that these morphological defects were not developmental (*SI Appendix*, Fig. S7*B* and Table S4).

We next tested whether expression of V30M TTR without the signal sequence (ΔSS) in FLP neurons with the *des-2* promoter

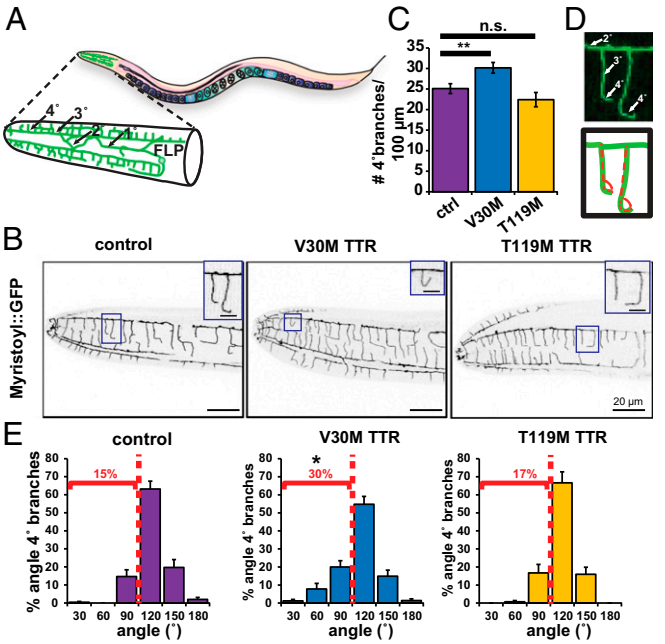

Fig. 5. Defective dendritic morphology of V30M TTR sensory neurons. (*A*) Schematic of the morphology of an FLP sensory neuron. Dendrites: 1°: primary; 2°: secondary; 3°: tertiary; 4°: quaternary. (*B*) Representative confocal images of the head region of a day-1 adult animal showing the contour of FLP neurons as delineated by *des-2p*::Myristoyl::GFP with same orientation as in *A*. *Insets* show enlargements of quaternary dendritic branches. Inverted images shown. (*C*) Quantification of the FLP dendrites (mean ± SEM). n = 20 animals per strain. $^{**}P < 0.01$, permutation t test. n.s., not significant. (*D*) Angles measured in *E*. (*E*) Histograms of the proportion of angular branches with a deviation greater than 0° in adult day-1 animals. $^{*}P < 0.025$; two-sample Kolmogorov–Smirnov test comparing angles of V30M TTR and control/T119M TTR. See also *SI Appendix*, Fig. S7 and Tables S3 and S4.

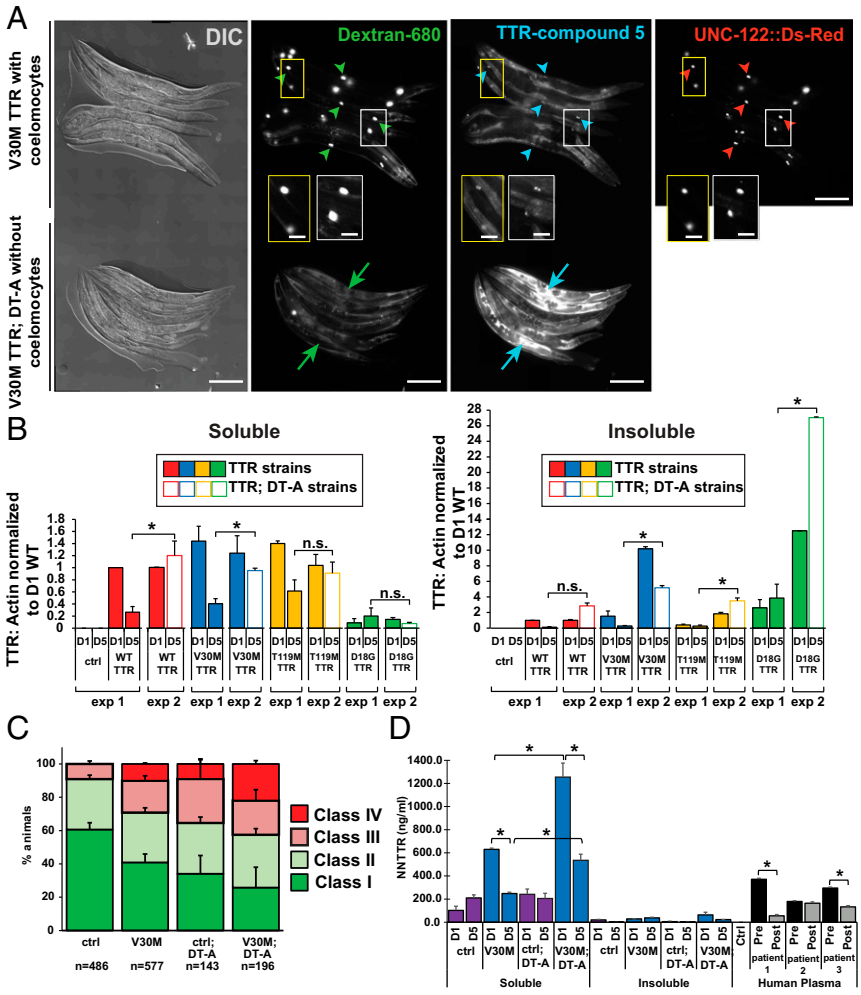

Fig. 6. Inhibition of TTR degradation exacerbates TTR cell-nonautonomous neuronal proteotoxicity. (*A*) Representative images showing day-2 adult V30M TTR transgenic animals with (V30M TTR; $n = 15$) and without (V30M TTR: DT-A; $n = 21$) coelomocytes. Coelomocytes in V30M TTR animals were visualized with a UNC-122::Ds-Red marker, but V30M TTR; DT-A animals did not have the UNC-122::Ds-Red marker. Arrowheads point to representative coelomocytes. Arrows point to body cavity fluorescence. *Insets* show enlargements. (Scale bars: 200 μm.) See also *SI Appendix*, Fig. S9 and Table S5. (*B*) Soluble (*Left*) and insoluble (*Right*) TTR protein levels from lysate fractions of synchronized day-1 (D1) and day-5 (D1 and D5) animals. Exp 1: Data are the same as shown in Fig. 1 *B* and *C* for TTR: actin levels of TTR (D5) animals. Exp 2: TTR: actin levels of TTR (D1) and TTR; DT-A (D5) animals. (*C*) Thermal-avoidance response. Data are representative of at least two independent experiments (mean ± SEM). See *SI Appendix*, Fig. S10 and Table S6. ctrl, control. (*D*) NN TTR oligomer levels by a sandwich ELISA in lysates of D1 and D5 adult animals. Three human patient samples before and after tafamidis treatment were included as positive controls for this assay. Data are shown as mean ± SEM, $n = 3$ for all panels, $^*P < 0.005$, Student's *t* test; ctrl, control.

(36) could drive the TTR nociception-sensing defects (Fig. 4). Nociception was not impaired in day-1 *des-2p*::V30MΔSS TTR animals (Fig. 4*B*), suggesting that V30M TTR expression in FLP neurons is not sufficient to impair nociception.

To test whether V30M TTR toxicity affects other neurons, we evaluated a subcellular phenotype in ALM, a set of mechanosensory neurons involved in soft-touch sensing (37). As mitochondria are critical for neuronal function, and their altered dynamics have been shown to be a key early pathological feature of most neurodegenerative diseases (38), we imaged and quantitated the size of these organelles inside ALM axons. Mitochondrial length was significantly decreased in V30M TTR animals compared with non-TTR control and T119M animals (*SI Appendix*, Fig. S8). These data suggest that secreted V30M TTR is not specifically toxic to sensory pain-sensing neurons but is also toxic to those involved in mechanosensation. Taken together, our data show that V30M TTR proteotoxicity impairs neuronal function in a cell-nonautonomous manner by targeting pathways that regulate the proper structure and function of pain-sensing and mechanosensory neurons.

TTR Clearance by Distal Cells Exacerbates TTR Proteotoxicity in Neurons. Our data show that TTR tetramers secreted from the body-wall muscle into the body cavity are taken up by coelomocytes (Fig. 2). As coelomocytes are lysosomal-degradative cells (28), we reasoned that if TTR was degraded in coelomocytes, then modulation of coelomocyte-mediated TTR degradation would affect the level of TTR proteotoxicity. To first test if TTR was degraded in coelomocytes, we genetically ablated these cells by crossing the TTR transgenic animals to a strain expressing a diphtheria toxin mutant, DT-A(E148D), under a coelomocyte-specific promoter and measured TTR levels (28). We confirmed the absence or significant reduction of coelomocytes in DT-A(E148D) animals (*SI Appendix*, Fig. S9 *A* and *B* and Table S5). Previous studies showed that ablation of coelomocytes resulted in the accumulation of fluid-phase markers in the body cavity due to a lack of uptake and degradation (28). To test for coelomocyte ablation in TTR; DT-A strains, we injected the body cavity with soluble A680-fluorescent dextran (3,000 MW) and immediately treated them with **CMPD5** (10 μM) to convert native TTR to TTR-(**CMPD5**)$_2$ tetrameric conjugates, as

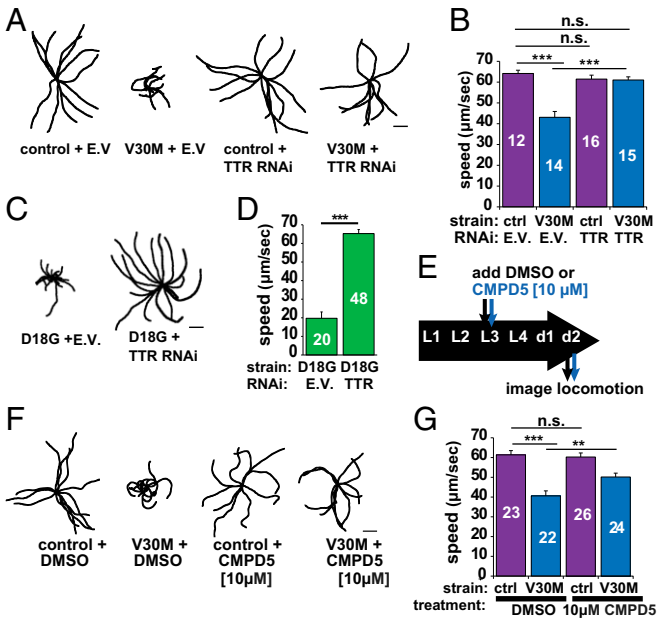

Fig. 7. Reduction or stabilization of TTR levels improves TTR-mediated locomotion impairments. (*A*) Representative 40-s locomotion trajectories of adult day-1 animals quantified in *B*. The starting points for each trajectory were aligned in the middle. (*B*) Comparison of locomotion rates in the indicated strains. The number of animals analyzed is shown inside the bars. See also *SI Appendix*, Fig. S11. (*C*) Representative 40-s locomotion trajectories of the indicated strains. (*D*) Locomotion rates of the animals plotted in *C*. (*E*) Schematic of the timeline for the locomotion and **CMPD5** treatment assay. (*F*) Representative 40-s trajectories of the indicated strains. (*G*) Locomotion rates for 2-d-old strains plotted in *F*. Plots show mean ± SEM, $^{**}P < 0.005$, $^{***}P < 0.001$, by Student's *t* test. E.V., empty vector; n.s., not significant. (Scale bars: 2 mm.)

described above (Fig. 2 *B* and *C*). A680-dextran as well as TTR–(**CMPD5**)$_2$ conjugates accumulated in coelomocytes in non–DT-A animals but accumulated throughout the body cavity in TTR; DT-A animals, suggesting that muscle-secreted TTR (WT TTR, V30M TTR and T119M TTR) was normally taken up from the body cavity and degraded in these cells (Fig. 6*A* and *SI Appendix*, Fig. S9 *C* and *F*). Neither non-TTR control animals nor D18G TTR; DT-A animals treated with **CMPD5** produced any significant TTR–(**CMPD5**)$_2$ conjugate signal (*SI Appendix*, Fig. S9 *E* and *D*). Next, to test whether ablation of coelomocytes resulted in decreased TTR degradation, we characterized TTR protein levels in animals with and without coelomocytes. Western blots of the soluble and insoluble TTR fractions of lysates from TTR; DT-A age-synchronized animals showed that adult 5-d-old animals without coelomocytes had increased TTR protein levels compared with animals with coelomocytes (Fig. 6*B*). This shows that ablation of coelomocytes resulted in a significant decrease in TTR degradation and in the accumulation of higher levels of TTR tetramers and insoluble TTR in the body cavity of aging animals.

Next, to determine whether decreasing TTR tetramer degradation cell nonautonomously increased TTR proteotoxicity in neurons, we tested for thermal avoidance in V30M TTR; DT-A animals. A significantly higher percentage of the V30M; DT-A animals (22 ± 2%; $n = 43$) failed to respond to noxious heat (class IV) compared with non-TTR control; DT-A (9.1 ± 2.5%; $n = 12$) or V30M TTR animals with coelomocytes (10 ± 0.6%; $n = 41$). Thus, reduced TTR degradation resulted in enhanced TTR neuronal defects (Fig. 6*C* and *SI Appendix*, Table S6).

To test whether the higher number of nonresponsive V30M; DT-A animals correlated with an increase in the amount of NN V30M TTR oligomers, we measured NN TTR oligomer load via ELISA, as described above (Fig. 3*D*). The NN TTR oligomer aggregate load was significantly increased in the soluble fraction of lysates of day-1 and day-5 adult V30M TTR; DT-A animals compared with that of V30M TTR animals (Fig. 6*D*). These data suggest that the additional impairment of neuronal nociception in V30M TTR; DT-A animals correlated with the increased soluble TTR tetramers and oligomers (Fig. 6 *A* and *B*). No significant increase in the amount of insoluble NN TTR oligomers was observed in V30M TTR; DT-A animals compared with V30M TTR animals, suggesting that soluble NN oligomers could be responsible for the heightened thermal-avoidance defect in animals without coelomocytes. Taken together, these data show that removal of degradative cells distal to the original site of V30M TTR expression can increase TTR tetramer levels throughout the body cavity by decreasing TTR protein turnover. These results suggest that enhanced TTR degradation at distal sites could ameliorate neuronal TTR phenotypes.

Reduction or Small Molecule Stabilization of Native TTR Levels Improves TTR-Mediated Locomotion Impairments and Decreases Oligomeric Aggregate Load. As neurons or possibly muscles are affected in our models, we next assessed whether expressing V30M TTR led to movement impairments. Expression of V30M TTR resulted in impaired locomotion as measured by decreased displacement and velocities compared with non-TTR controls, and TTR RNAi rescued this phenotype (Fig. 7 *A* and *B* and *SI Appendix*, Fig. S4). These motility defects could be the result of impaired muscle and/or neuronal function (39, 40). To test whether V30M TTR motility could be affected as a result of muscle dysfunction, we performed TTR RNAi in the D18G strain in which we observed no evidence of TTR secretion (Fig. 2*C*). One-day-old D18G TTR animals exhibited a pronounced uncoordinated (Unc) phenotype, which was rescued by RNAi against TTR (Fig. 7 *C* and *D*). These data suggest that D18G TTR proteotoxicity affects proteostasis in the muscle and results in its malfunction, although muscle morphology appeared unaffected (Fig. 2*A* and *SI Appendix*, Fig. S2). Thus, expression of V30M TTR could result in defects in locomotion due to TTR cell-autonomous impairment of muscle function, but this merits further scrutiny.

Next, we tested whether stabilizing TTR pharmacologically would ameliorate the TTR-dependent Unc phenotype. To stabilize the native TTR tetramer quaternary structure, we treated V30M TTR animals with **CMPD5**. In addition to being fluorogenic upon binding to and reacting with TTR (Fig. 2 *B* and *C*), **CMPD5** affords a hyperstable tetramer, which ameliorates FAP by preventing aggregation, similar to tafamidis (8, 30). We chose **CMPD5** as the kinetic stabilizer instead of tafamidis because **CMPD5** exhibits better solubility (41). Since V30M TTR oligomers were detected in day-1 adult animals (Fig. 3*C*), we initially treated L1, L3, L4, and day-1 animals with various concentrations of **CMPD5** to establish a therapeutic dose. We determined that 10 μM applied to L3 larvae produced a response without toxicity (Fig. 7*E* and *SI Appendix*, Fig. S11*A*). **CMPD5**-treated L3 V30M TTR larvae assessed at day 2 of adulthood exhibited significantly restored locomotion (51.3% rescue of mean speed) compared with nontreated animals (Fig. 7 *F* and *G*). These data show that *C. elegans* FAP models respond to treatment with a pharmacological kinetic stabilizer to ameliorate TTR-dependent phenotypes, likely as a result of the stabilization of TTR tetramers, as demonstrated in human FAP patient serum (31).

To test whether the rescued locomotion phenotype following treatment with **CMPD5** was the result of a decrease in the TTR oligomeric aggregate load, we measured NN TTR levels by ELISA in lysates of day-2 V30M TTR animals with or without **CMPD5**. We observed a significant reduction in NN V30M TTR levels only in the soluble fractions of V30M TTR strains without coelomocytes (*SI Appendix*, Fig. S11*C*), which we earlier showed had significantly increased NN TTR oligomer levels (Fig. 6*D*). These data suggest that the rescue of the locomotion phenotype with **CMPD5** could result from a decrease in the soluble NN TTR oligomer pool. Taken together, our data show that preventing TTR

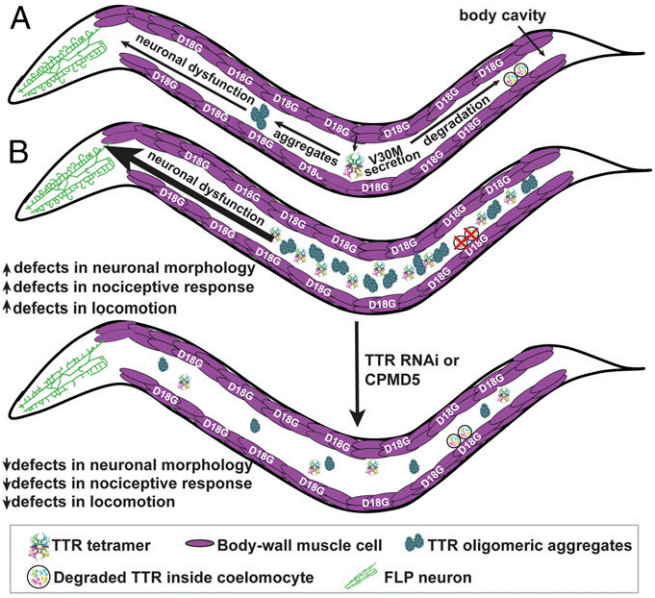

Fig. 8. TTR cell-nonautonomous clearance and proteotoxicity model. (*A*) Expression of V30M TTR in the body-wall muscle results in the secretion of this variant as tetramers into the body cavity where V30M TTR is subsequently endocytosed by coelomocytes for degradation. D18G TTR remains in the muscle where it generates cell-autonomous dysfunction. TTR oligomers are generated whose presence correlates with impaired nociceptive response and with morphological abnormalities in the sensory neurons involved in this response. (*B*) Modulation of TTR-dependent cell-nonautonomous proteotoxicity can be accomplished by modifications to TTR degradation at distal sites (coelomocytes). Ablating coelomocytes results in increased TTR-dependent proteotoxicity. Reduction of TTR levels at the source cell autonomously by RNAi or nonautonomously by a small molecule (**CMPD5**) reduces TTR-dependent proteotoxicity.

aggregation, either by reducing TTR levels via RNAi or by slowing tetramer dissociation with a kinetic stabilizer (i.e., **CMPD5**), can rescue TTR-mediated locomotion defects, showing that the locomotion phenotype results from TTR aggregation.

Discussion

A Model to Study Cell-Nonautonomous Proteostatic Mechanisms for Modulating Aggregate-Prone Toxicity. Previous *C. elegans* proteinopathy models expressing human disease-linked aggregation-prone proteins specifically in the body-wall muscle, neurons, or intestine exhibited uniquely cell-autonomous tissue-specific toxicity (1). These included degenerative disease models expressing amyloid beta (Aβ) (29), poly-glutamine expansion proteins (42, 43), α-synuclein (44), WT or mutant prion protein (45), various tau variants (46), TDP-43 (47), an Ig light chain (48), and α1-antitrypsin (49). Recent observations in cell-culture models and mice have demonstrated that proteotoxicity by misfolded proteins in AD, PD, amyotrophic lateral sclerosis, Huntington's disease, and the prion diseases also appear to have cell-nonautonomous components that involve damage of tissues or cells other than those expressing the aggregation-prone, disease-associated proteins (50–52). However, the cell-nonautonomous pathways of neurodegeneration remain incompletely understood for all human amyloid diseases, in part due to the lack of models that faithfully recapitulate *in trans* toxicity. *C. elegans* have been used previously to model and characterize the cell-nonautonomous role of neuronal signaling in the impairment and restoration of proteostasis across tissues. Specifically, null mutations in *unc-30*, a transcription factor that regulates the synthesis of the inhibitory neurotransmitter GABA, caused the premature appearance of polyQ35 aggregates and an imbalance in proteostasis of postsynaptic muscle cells (53). Moreover, down-regulation of neuronally expressed *gei-11* (54), a Myb-family factor that regulates L-type AChR, increased cholinergic receptor activity at the neuromuscular junction and suppressed toxicity and protein misfolding in postsynaptic muscle cells, suggesting an effect of cholinergic signaling on muscle homeostasis (55). In addition, cell-to-cell spreading of protein aggregates has been modeled previously in *C. elegans* by expressing the cytosolic Sup35 prion NM domain from yeast in the body-wall muscle (56). Also, human α-synuclein aggregates in *C. elegans* were shown to transfer between neurons (57). Thus, these promising transgenic models could contribute to elucidating cell-nonautonomous mechanisms as well as the effects of cell-to-cell transfer of aggregate-prone toxicity, which remain unclear for all human aggregate- and spread-prone misfolding proteins.

In the TTR amyloid diseases, cell-nonautonomous toxicity is the default mechanism, thus affording the possibility to study mechanisms of toxicity directly *in trans*. The TTR models studied herein recapitulate TTR cell-nonautonomous neurotoxicity and show clear cell-nonautonomous disease model phenotypes in *C. elegans*. Our model (Fig. 8) posits that disease-prone WT TTR and V30M TTR tetramers are secreted from the muscle into the body cavity where they are endocytosed by coelomocytes for degradation, a process that competes with NN TTR oligomer generation (i.e., misfolding and aggregation). Increases in NN V30M TTR oligomers correlate with compromised FLP sensory neuronal structure and function, as well as with locomotion defects, although other aggregated TTR structures could also contribute. D18G TTR was not efficiently secreted from the muscle, forming intracellular aggregates and exhibiting strong paralysis. We hypothesize that an overloaded ERAD system was unable to degrade D18G TTR in the muscle, demonstrating that TTR toxicity could also act cell autonomously.

The presence of protein aggregates in neurodegenerative diseases is a key indicator of disrupted organismal proteostasis (58, 59). Since increasing the NN V30M TTR oligomer load by inhibiting cell-nonautonomous TTR degradation by coelomocyte ablation significantly exacerbated the nociceptive defect in V30M TTR animals, our studies suggest that the NN V30M TTR oligomers contributed to the degenerative phenotype (Fig. 8). A conclusion from our study is that adjusting TTR tetramer concentration both cell autonomously (by RNAi to decrease TTR mRNA in the muscle) and cell nonautonomously (by coelomocyte ablation) can modulate cell-nonautonomous TTR proteotoxicity. Moreover, TTR tetramer kinetic stabilization by a small molecule reduced TTR oligomers and rescued V30M-mediated locomotion defects (Fig. 7 and *SI Appendix*, Fig. S11). These data suggest that *C. elegans* TTR models recapitulated human TTR aggregation pathways, as RNAi and kinetic stabilizers slow or stop degeneration in humans. The notion that protein-aggregate formation and proteostasis can be modulated by altering the levels of aggregate precursors in either the TTR-secreting cells or in distal cells primarily responsible for TTR degradation could provide avenues for possible therapeutic interventions. As coelomocyte degradation is autophagosomal (60), our data suggest that modulating autophagic activity cell nonautonomously could regulate TTR tetramer and oligomer levels and reduce NN TTR-mediated neurotoxicity. The liver, muscle, and skin have been shown to be the major sites of TTR degradation in rats, with no detectable degradation occurring in nervous tissue (61). Thus, the activation of autophagy or analogous lysosomal degradation mechanisms in these tissues should be considered as a strategy for treating the TTR amyloidoses and other amyloid diseases.

Cell-Nonautonomous Impairment of Neuronal Structure and Function by Toxic Oligomeric TTR. In this study, we modeled V30M TTR-associated FAP cell-nonautonomous neurotoxicity, a feature not recapitulated in previously published *Drosophila* or murine models (22–24). Consistent with the observed defects in nociceptive sensing, extracellular V30M TTR resulted in defective FLP dendritic branch extension and in ectopic branching that appeared to be due to degenerative processes rather than developmental defects. As

nociceptive sensing was only partially impaired in V30M TTR animals, it is possible that TTR proteotoxicity primarily impaired FLP function, whereas AFD, the other neurons responsible for nociception (30, 32), were less affected; however, this needs to be evaluated further. Putative sensory neuron selectivity would suggest a specific TTR-targeting mechanism. However, V30M TTR toxicity appeared not to be selective for nociceptive neurons, as we observed defective subcellular phenotypes in mechanosensory neurons (mitochondrial size). The extent of putative *in trans* deficits in other neurons merits future investigation.

It is unclear whether TTR toxicity is imparted via direct neuronal internalization of TTR, but previous in vitro studies showed that TTR can be endocytosed into sensory neurons (62, 63). Our data show that animals expressing V30M TTR inside FLP neurons have a normal nociceptive response, demonstrating that TTR expression inside neurons may not be sufficient to drive toxicity. Thus, unknown extracellular pathways could mediate the effects of TTR toxicity. Another possibility is that V30M TTR could internalize in other neurons and drive toxicity in FLP sensory neurons via direct or indirect neuron-to-neuron interactions. In either case, our data point toward neuronal toxicity occurring as a result of cell-nonautonomous mechanisms, as nociception was not affected in the nonsecreting D18G TTR animals.

The observed cell-nonautonomous neuronal phenotypes of V30M TTR animals suggest that affected neurons experienced increased cell-nonautonomous proteostatic stress and a heightened stress response. How a TTR-mediated proteotoxic cell-nonautonomous stress response might be regulated remains unknown. Importantly, *in trans* mechanisms have been shown to play a role in the regulation of stress response pathways in *C. elegans* and mammals (64–67). At the organismal level in *C. elegans*, the heat-shock response (HSR) is regulated in somatic nonneuronal tissues by the AFD thermosensory neurons, which, in addition to regulating nociception, also normally modulate responses to ambient temperature to adjust thermotaxis (68). While it is unknown whether AFD function is compromised in V30M TTR animals, it is possible, because this neuron is involved in nociception (34), that a putative defective AFD function could result in an impaired HSR. If this response is impaired in V30M TTR animals, the ability of this neuron to mount an HSR could lead to the misregulation of organismal-level proteostasis. Interestingly, mutations affecting AFD function (*tax-4*, *gcy-8*, and *gcy-23*) both impair the ability to mount an HSR and display a diminished nociceptive response (68).

TTR toxicity also resulted in overbranching dendritic morphology. Notably, previous studies showed that, upon aging, the *C. elegans* nervous system exhibits significant age-dependent ectopic branching rather than neuronal cell death (69, 70). The underlying mechanisms of age-dependent aberrant ectopic branches in WT animals in these earlier studies are still unclear, but these features correlated with the age-related deterioration of synaptic structure and function. Indeed, early-disease pathology in humans is characterized by neuronal alterations, including significant dendritic pathology (71), that precede cell death. Thus, the *C. elegans* dendritic arborization phenotypes observed herein correlate with age-dependent neuronal deterioration and are already apparent in young-adult TTR animals. Thus, the models presented here seem poised to facilitate the elucidation of the mechanisms of TTR aggregation-dependent neurodegeneration. Moreover, these models could be key for scrutinizing the basis of tissue tropism in the TTR amyloidoses, e.g., neuronal versus cardiac degeneration. Due to its analogy to the vertebrate heart, the rhythmic contractile activity of the pharynx in the transgenic *C. elegans* TTR models could be used to characterize the basis of TTR cardiac tissue toxicity in TTR cardiomyopathies, as accomplished previously in other amyloidosis models (48). The ability to probe for tissue-specific mechanisms of toxicity and do genetic screens in *C. elegans* should help identify the genetic and molecular pathways by which peripheral tissues, including heart or sensory neurons, are selectively impaired in the TTR amyloidoses.

Materials and Methods

Detailed methods and a complete list of strains and constructs used in this study are provided in *SI Appendix, SI Materials and Methods*.

Native PAGE Gel Analysis for Detection of TTR Oligomers. Soluble lysate and the insoluble pellet were obtained from synchronized *C. elegans* as described in *SI Appendix, SI Materials and Methods*. The samples were resolved on Novex NativePAGE 3–12% Bis-Tris protein gels (Invitrogen) and probed with the MDX102 antibody against oligomeric TTR after transfer to a nitrocellulose membrane. Validation of antibodies used in this assay is reported in *SI Appendix, SI Materials and Methods* under *Antibodies Against Oligomeric TTR* (*SI Appendix*, Fig. S3 *A* and *B*).

Quantification of NN TTR Levels in Vitro by ELISA. NN TTR levels were quantitated using a sandwich ELISA developed by Misfolding Diagnostics, Inc. (patent WO2014/124334A2). Validation of antibodies used in this assay is reported in *SI Appendix, SI Materials and Methods* under *Antibodies Against Oligomeric TTR* (*SI Appendix*, Fig. S3 *A* and *B*). The lysates were obtained as mentioned above. Each sample used in the assay contained 2.4 μg of the total protein. A misfolded form of recombinant TTR protein was used to generate the standard curve.

Thermal-Avoidance Assay for Nociception. The thermal-avoidance assay was done on day-1 adult animals, and their response to noxious heat was scored in one of the four categories, as published previously (*SI Appendix, SI Materials and Methods*) (33).

Locomotion Assay and Worm-Tracking Analysis. Individual day-2 adult animals' movement trajectories were recorded for a duration of 40 s using a Stemi 508 microscope (Zeiss) with a SwiftCam2 camera and imaging software (Swift). All movies were analyzed using the wrMTrck plugin for ImageJ to obtain average speed and representative tracks of each of the trajectories (*SI Appendix, SI Materials and Methods*) (72).

ACKNOWLEDGMENTS. We thank J. Genereux, C. Monteiro, J. Chen, Y. Eisele, and G. Dendle (The Scripps Research Institute) for assistance with UPLC experiments and providing recombinant TTR; C. Link (University of Colorado at Boulder), C. Bargmann (The Rockefeller University), H. Fares (University of Arizona), and the Caenorhabditis Genetics Center for strains; S. Srinivasan (The Scripps Research Institute) and M. Hansen (Sanford Burnham Prebys Medical Discovery Institute) for reagents; S. Wolff and P. Frankino (University of California, Berkeley) for preliminary analyses; and M. Hansen, M. Petrascheck, C. Fearns, L. Wiseman, and members of the S.E.E. laboratory for advice and critical feedback on the manuscript. This work was supported in part by NIH-National Institute on Aging Grant 1R01AG038664, by the Glenn Foundation for Medical Research Glenn Award for Research in Biological Mechanisms of Aging, by a New Scholar in Aging Award from the Lawrence Ellison Foundation, and by Baxter Family Foundation awards (to S.E.E.); and by NIH-National Institute of Diabetes and Digestive and Kidney Disease Grant DK046335 (to J.W.K.). K.M. and E.R.G. were supported by the George E. Hewitt Foundation for Medical Research. M.A.-F. was supported by Fundação para a Ciência e Tecnologia Fellowship SFRH/BD/101352/2014, and J.F.P. was supported by the Swedish Research Council. V.P. is funded by NIH Grant R01 AG 050653. F.K.O. was supported by a graduate student fellowship from the Developmental Studies Hybridoma Bank.

1. Nussbaum-Krammer CI, Morimoto RI (2014) *Caenorhabditis elegans* as a model system for studying non-cell-autonomous mechanisms in protein-misfolding diseases. *Dis Model Mech* 7:31–39.
2. Goedert M, Falcon B, Clavaguera F, Tolnay M (2014) Prion-like mechanisms in the pathogenesis of tauopathies and synucleinopathies. *Curr Neurol Neurosci Rep* 14:495.
3. Holmgren G, et al. (1991) Biochemical effect of liver transplantation in two Swedish patients with familial amyloidotic polyneuropathy (FAP-met30). *Clin Genet* 40:242–246.
4. Blake CC, Geisow MJ, Oatley SJ, Rérat B, Rérat C (1978) Structure of prealbumin: Secondary, tertiary and quaternary interactions determined by Fourier refinement at 1.8 A. *J Mol Biol* 121:339–356.
5. Monaco HL, Rizzi M, Coda A (1995) Structure of a complex of two plasma proteins: Transthyretin and retinol-binding protein. *Science* 268:1039–1041.
6. Bartalena L, Robbins J (1992) Variations in thyroid hormone transport proteins and their clinical implications. *Thyroid* 2:237–245.
7. Coelho T, et al. (1993) A strikingly benign evolution of FAP in an individual found to be a compound heterozygote for two TTR mutations: TTR MET 30 and TTR MET 119. *J Rheumatol* 20:179.
8. Johnson SM, Connelly S, Fearns C, Powers ET, Kelly JW (2012) The transthyretin amyloidoses: From delineating the molecular mechanism of aggregation linked to pathology to a regulatory-agency-approved drug. *J Mol Biol* 421:185–203.

9. Schonhoft JD, et al. (2017) Peptide probes detect misfolded transthyretin oligomers in plasma of hereditary amyloidosis patients. *Sci Transl Med* 9:eaam7621.
10. Saraiva MJ, Costa PP, Birken S, Goodman DS (1983) Presence of an abnormal transthyretin (prealbumin) in Portuguese patients with familial amyloidotic polyneuropathy. *Trans Assoc Am Physicians* 96:261–270.
11. Eisele YS, et al. (2015) Targeting protein aggregation for the treatment of degenerative diseases. *Nat Rev Drug Discov* 14:759–780.
12. Olzscha H, et al. (2011) Amyloid-like aggregates sequester numerous metastable proteins with essential cellular functions. *Cell* 144:67–78.
13. Escusa-Toret S, Vonk WIM, Frydman J (2013) Spatial sequestration of misfolded proteins by a dynamic chaperone pathway enhances cellular fitness during stress. *Nat Cell Biol* 15:1231–1243.
14. Voisine C, Pedersen JS, Morimoto RI (2010) Chaperone networks: Tipping the balance in protein folding diseases. *Neurobiol Dis* 40:12–20.
15. Caughey B, Lansbury PT (2003) Protofibrils, pores, fibrils, and neurodegeneration: Separating the responsible protein aggregates from the innocent bystanders. *Annu Rev Neurosci* 26:267–298.
16. Sekijima Y, et al. (2005) The biological and chemical basis for tissue-selective amyloid disease. *Cell* 121:73–85.
17. Saraiva MJ (1995) Transthyretin mutations in health and disease. *Hum Mutat* 5: 191–196.
18. Coelho T, Maurer MS, Suhr OB (2013) THAOS–The Transthyretin Amyloidosis Outcomes Survey: Initial report on clinical manifestations in patients with hereditary and wild-type transthyretin amyloidosis. *Curr Med Res Opin* 29:63–76.
19. Hammarström P, et al. (2003) D18G transthyretin is monomeric, aggregation prone, and not detectable in plasma and cerebrospinal fluid: A prescription for central nervous system amyloidosis? *Biochemistry* 42:6656–6663.
20. Vidal R, et al. (1996) Meningocerebrovascular amyloidosis associated with a novel transthyretin mis-sense mutation at codon 18 (TTRD 18G). *Am J Pathol* 148:361–366.
21. Westermark P, Sletten K, Johansson B, Cornwell GG, 3rd (1990) Fibril in senile systemic amyloidosis is derived from normal transthyretin. *Proc Natl Acad Sci USA* 87: 2843–2845.
22. Buxbaum JN (2009) Animal models of human amyloidoses: Are transgenic mice worth the time and trouble? *FEBS Lett* 583:2663–2673.
23. Berg I, Thor S, Hammarström P (2009) Modeling familial amyloidotic polyneuropathy (Transthyretin V30M) in Drosophila melanogaster. *Neurodegener Dis* 6:127–138.
24. Pokrzywa M, Dacklin I, Hultmark D, Lundgren E (2007) Misfolded transthyretin causes behavioral changes in a Drosophila model for transthyretin-associated amyloidosis. *Eur J Neurosci* 26:913–924.
25. Jiang X, Kelly JW, Chapman J (2014) US Patent WO2014124334A2.
26. Sousa MM, Cardoso I, Fernandes R, Guimarães A, Saraiva MJ (2001) Deposition of transthyretin in early stages of familial amyloidotic polyneuropathy: Evidence for toxicity of nonfibrillar aggregates. *Am J Pathol* 159:1993–2000.
27. Choi S, Connelly S, Reixach N, Wilson IA, Kelly JW (2010) Chemoselective small molecules that covalently modify one lysine in a non-enzyme protein in plasma. *Nat Chem Biol* 6:133–139.
28. Fares H, Greenwald I (2001) Genetic analysis of endocytosis in Caenorhabditis elegans: Coelomocyte uptake defective mutants. *Genetics* 159:133–145.
29. Link CD (1995) Expression of human beta-amyloid peptide in transgenic Caenorhabditis elegans. *Proc Natl Acad Sci USA* 92:9368–9372.
30. Baranczak A, et al. (2015) A fluorogenic aryl fluorosulfate for intraorganellar transthyretin imaging in living cells and in Caenorhabditis elegans. *J Am Chem Soc* 137: 7404–7414.
31. Rappley I, et al. (2014) Quantification of transthyretin kinetic stability in human plasma using subunit exchange. *Biochemistry* 53:1993–2006.
32. Adamla F, Ignatova Z (2015) Somatic expression of unc-54 and vha-6 mRNAs declines but not pan-neuronal rgef-1 and unc-119 expression in aging Caenorhabditis elegans. *Sci Rep* 5:10692.
33. Wittenburg N, Baumeister R (1999) Thermal avoidance in Caenorhabditis elegans: An approach to the study of nociception. *Proc Natl Acad Sci USA* 96:10477–10482.
34. Liu S, Schulze E, Baumeister R (2012) Temperature- and touch-sensitive neurons couple CNG and TRPV channel activities to control heat avoidance in Caenorhabditis elegans. *PLoS One* 7:e32360.
35. Albeg A, et al. (2011) C. elegans multi-dendritic sensory neurons: Morphology and function. *Mol Cell Neurosci* 46:308–317.
36. Treinin M, Gillo B, Liebman L, Chalfie M (1998) Two functionally dependent acetylcholine subunits are encoded in a single Caenorhabditis elegans operon. *Proc Natl Acad Sci USA* 95:15492–15495.
37. Chalfie M, Sulston J (1981) Developmental genetics of the mechanosensory neurons of Caenorhabditis elegans. *Dev Biol* 82:358–370.
38. Gao J, et al. (2017) Abnormalities of mitochondrial dynamics in neurodegenerative diseases. *Antioxidants* 6:E25.
39. Morley JF, Brignull HR, Weyers JJ, Morimoto RI (2002) The threshold for polyglutamine-expansion protein aggregation and cellular toxicity is dynamic and influenced by aging in *Caenorhabditis elegans*. *Proc Natl Acad Sci USA* 99: 10417–10422.
40. Wang J, et al. (2009) An ALS-linked mutant SOD1 produces a locomotor defect associated with aggregation and synaptic dysfunction when expressed in neurons of *Caenorhabditis elegans*. *PLoS Genet* 5:e1000350.
41. Grimster NP, et al. (2013) Aromatic sulfonyl fluorides covalently kinetically stabilize transthyretin to prevent amyloidogenesis while affording a fluorescent conjugate. *J Am Chem Soc* 135:5656–5668.
42. Brignull HR, Morley JF, Morimoto RI (2007) The stress of misfolded proteins: C. elegans models for neurodegenerative disease and aging. *Adv Exp Med Biol* 594: 167–189.
43. Parker JA, Holbert S, Lambert E, Abderrahmane S, Néri C (2004) Genetic and pharmacological suppression of polyglutamine-dependent neuronal dysfunction in Caenorhabditis elegans. *J Mol Neurosci* 23:61–68.
44. Lakso M, et al. (2003) Dopaminergic neuronal loss and motor deficits in *Caenorhabditis elegans* overexpressing human α-synuclein. *J Neurochem* 86:165–172.
45. Park KW, Li L (2008) Cytoplasmic expression of mouse prion protein causes severe toxicity in *Caenorhabditis elegans*. *Biochem Biophys Res Commun* 372:697–702.
46. Hannan SB, Dräger NM, Rasse TM, Voigt A, Jahn TR (2016) Cellular and molecular modifier pathways in tauopathies: The big picture from screening invertebrate models. *J Neurochem* 137:12–25.
47. Ash PE, et al. (2010) Neurotoxic effects of TDP-43 overexpression in C. elegans. *Hum Mol Genet* 19:3206–3218.
48. Diomede L, et al. (2014) A Caenorhabditis elegans-based assay recognizes immunoglobulin light chains causing heart amyloidosis. *Blood* 123:3543–3552.
49. Cummings EE, et al. (2015) Deficient and null variants of SERPINA1 are proteotoxic in a Caenorhabditis elegans model of α1-antitrypsin deficiency. *PLoS One* 10:e0141542.
50. Ilieva H, Polymenidou M, Cleveland DW (2009) Non-cell autonomous toxicity in neurodegenerative disorders: ALS and beyond. *J Cell Biol* 187:761–772.
51. Brundin P, Melki R, Kopito R (2010) Prion-like transmission of protein aggregates in neurodegenerative diseases. *Nat Rev Mol Cell Biol* 11:301–307.
52. Marchetto MC, et al. (2008) Non-cell-autonomous effect of human SOD1 G37R astrocytes on motor neurons derived from human embryonic stem cells. *Cell Stem Cell* 3:649–657.
53. Garcia SM, Casanueva MO, Silva MC, Amaral MD, Morimoto RI (2007) Neuronal signaling modulates protein homeostasis in Caenorhabditis elegans post-synaptic muscle cells. *Genes Dev* 21:3006–3016.
54. Silva MC, et al. (2011) A genetic screening strategy identifies novel regulators of the proteostasis network. *PLoS Genet* 7:e1002438.
55. Silva MC, Amaral MD, Morimoto RI (2013) Neuronal reprograming of protein homeostasis by calcium-dependent regulation of the heat shock response. *PLoS Genet* 9: e1003711.
56. Nussbaum-Krammer CI, Park KW, Li L, Melki R, Morimoto RI (2013) Spreading of a prion domain from cell-to-cell by vesicular transport in Caenorhabditis elegans. *PLoS Genet* 9:e1003351.
57. Tyson T, et al. (2017) Novel animal model defines genetic contributions for neuron-to-neuron transfer of α-synuclein. *Sci Rep* 7:7506.
58. Balch WE, Morimoto RI, Dillin A, Kelly JW (2008) Adapting proteostasis for disease intervention. *Science* 319:916–919.
59. Hartl FU, Bracher A, Hayer-Hartl M (2011) Molecular chaperones in protein folding and proteostasis. *Nature* 475:324–332.
60. Sun T, Wang X, Lu Q, Ren H, Zhang H (2011) CUP-5, the *C. elegans* ortholog of the mammalian lysosomal channel protein MLN1/TRPML1, is required for proteolytic degradation in autolysosomes. *Autophagy* 7:1308–1315.
61. Makover A, et al. (1988) Plasma transthyretin. Tissue sites of degradation and turnover in the rat. *J Biol Chem* 263:8598–8603.
62. Sousa MM, Saraiva MJ (2001) Internalization of transthyretin. Evidence of a novel yet unidentified receptor-associated protein (RAP)-sensitive receptor. *J Biol Chem* 276: 14420–14425.
63. Fleming CE, Mar FM, Franquinho F, Saraiva MJ, Sousa MM (2009) Transthyretin internalization by sensory neurons is megalin mediated and necessary for its neuritogenic activity. *J Neurosci* 29:3220–3232.
64. Blake MJ, Udelsman R, Feulner GJ, Norton DD, Holbrook NJ (1991) Stress-induced heat shock protein 70 expression in adrenal cortex: An adrenocorticotropic hormone-sensitive, age-dependent response. *Proc Natl Acad Sci USA* 88:9873–9877.
65. Fawcett TW, Sylvester SL, Sarge KD, Morimoto RI, Holbrook NJ (1994) Effects of neurohormonal stress and aging on the activation of mammalian heat shock factor 1. *J Biol Chem* 269:32272–32278.
66. Taylor RC, Dillin A (2013) XBP-1 is a cell-nonautonomous regulator of stress resistance and longevity. *Cell* 153:1435–1447.
67. Durieux J, Wolff S, Dillin A (2011) The cell-non-autonomous nature of electron transport chain-mediated longevity. *Cell* 144:79–91.
68. Prahlad V, Cornelius T, Morimoto RI (2008) Regulation of the cellular heat shock response in Caenorhabditis elegans by thermosensory neurons. *Science* 320:811–814.
69. Tank EM, Rodgers KE, Kenyon C (2011) Spontaneous age-related neurite branching in Caenorhabditis elegans. *J Neurosci* 31:9279–9288.
70. Toth ML, et al. (2012) Neurite sprouting and synapse deterioration in the aging Caenorhabditis elegans nervous system. *J Neurosci* 32:8778–8790.
71. Kweon JH, Kim S, Lee SB (2017) The cellular basis of dendrite pathology in neurodegenerative diseases. *BMB Rep* 50:5–11.
72. Nussbaum-Krammer CI, Neto MF, Brielmann RM, Pedersen JS, Morimoto RI (2015) Investigating the spreading and toxicity of prion-like proteins using the metazoan model organism *C. elegans*. *J Vis Exp,* 52321.